Studia Quaternaria, vol. 43 (2026): 17–32
DOI: 10.24425/sq.2026.158729

HYDROGEOCHEMICAL PROCESSES GOVERNING GROUNDWATER QUALITY IN A SEMI-ARID BASIN, NORTHEASTERN ALGERIA

Zouhir Boulgueraguer[1,2], Amel Maou[3,4], Riheb Hadji[3,4,*], Ismail Arif[4]

[1] *Department of Biotechnology, Faculty of Natural and Life Sciences, Ferhat Abbas University, Setif, Algeria; e-mail: (ZB) boulgueraguer@yahoo.fr*
[2] *Laboratory of Water Resource and Sustainable Development (REDD), Department of Geology, Faculty of Earth Sciences, Badji Mokhtar University, Annaba, Algeria*
[3] *Department of Earth Sciences, Institute of Architecture and Earth Sciences, Ferhat Abbas University, El Bez, Setif, 19000, Algeria; e-mails: (AM) amelmaou@gmail.com, (RH) hadjirihab@yahoo.fr*
[4] *Laboratory of Applied Research in Engineering Geology, Geotechnics, Water Sciences, and Environment, Ferhat Abbas University, El Bez, Setif, 19000, Algeria; e-mail: (IA) labo_geo@yahoo.fr*
* *corresponding author*

Abstract:
This study addresses the hydrogeochemical assessment of alluvial aquifers in a semi-arid region, where groundwater constitutes a critical resource for drinking supply and irrigated agriculture but is increasingly threatened by salinization and geogenic constraints. It investigates the hydrogeochemical characteristics and practical usability of groundwater from the Quaternary aquifer of the Bousselam Upstream River basin (BUR), northeastern Algeria. Forty-two groundwater samples were collected from fourteen wells during three monitoring campaigns conducted in 2020, 2022, and 2024 to capture spatial variability and short-term temporal evolution. Physicochemical parameters and major ions were analyzed following APHA standard methods, and hydrochemical facies were identified using Piper, Schoeller, Wilcox, and Riverside diagrams. Groundwater is mildly alkaline and moderately mineralized (EC:1154–1632 µS/cm), reflecting dominant water-rock interactions with limited anthropogenic influence. The prevailing Ca-Mg-SO_4-Cl and Ca-HCO_3 facies are controlled by carbonate and evaporite dissolution and ion-exchange processes. Total hardness values indicate predominantly hard to very hard water. Water Quality Index values (25–75) range from good to poor, while irrigation assessments classify most samples as S1C3, indicating low sodium hazard but elevated salinity. Beyond academic characterization, the results highlight practical constraints on long-term use and support the need for targeted management strategies to sustain groundwater use for drinking and irrigation.

Key words: Quaternary aquifer, Water Quality Index, Drinking potability, Irrigation suitability, Bousselam Upstream River.

Manuscript received 10 November 2025, accepted 3 February 2026

INTRODUCTION

Water quality deterioration has emerged as a pressing environmental challenge in arid and semi-arid regions worldwide, with particularly acute implications across the Middle East and North Africa (MENA). In these water-scarce regions, both surface and groundwater resources constitute the backbone of domestic supply, agricultural production, and industrial activities. The protection and sustainable management of these resources are therefore critical for public health, ecosystem stability, and socio-economic development (Ouyang, 2005; Kazi *et al.*, 2009). However, a combination of natural processes (such as mineral weathering, hydroclimatic variability, and seasonal recharge fluctuations) and anthropogenic pressures, including urban expansion, industrial effluents, intensive agricultural practices, and insufficient wastewater treatment, has intensified water quality degradation over recent decades. Consequently, a detailed understanding of the spatial and temporal variability of hydrochemical parameters and the geochemical mechanisms controlling solute distribution is essential to ensure the long-term sustainability of water resources in these vulnerable environments.

Hydrogeochemical investigations offer a robust framework to elucidate interactions between groundwater and surrounding lithological formations, including ion exchange processes, mineral dissolution, and precipitation dynamics (Giridharan *et al.*, 2010; Subramani *et al.*, 2010). These studies enable differentiation between natural geochemical signatures and anthropogenic influences, providing a scientific basis to assess the suitability of water for domestic consumption, irrigation, and industrial applications (Möller *et al.*, 2009). Across North Africa, research has highlighted the significant impacts of industrial and agricultural activities on water quality. For instance, Hamed *et al.* (2023, 2024a, b, 2025a, b) examined phosphate industry effluents in the Gafsa Basin, Tunisia, while Brahmi *et al.* (2021), Nekkoub *et al.* (2020), and Charouf *et al.* (2025) applied multivariate statistical analyses and GIS-based approaches to identify dominant factors shaping groundwater chemistry. Similarly, Benmarce *et al.* (2024) demonstrated the effectiveness of the Water Quality Index (WQI) as an integrative tool for communicating complex hydrochemical information and evaluating potability.

Originally developed by Horton (1965) and refined by Brown *et al.* (1970), the WQI condenses multiple water quality indicators into a single, interpretable metric. Global adaptations (including the NSFWQI (U.S.), CCMEWQI (Canada), and BCWQI (British Columbia)) facilitate standardized comparisons across diverse hydroclimatic and socio-environmental contexts, underscoring the index's international applicability (Kannel *et al.*, 2007; Chaturvedi and Bassin, 2010).

While earlier hydrogeochemical investigations in North Africa and the wider MENA region have largely relied on single-campaign datasets, site-specific pollution screening, or the descriptive use of water quality indices (Ncibi *et al.*, 2020; Bensoltane *et al.*, 2021; Benmarce *et al.*, 2023; Chougar *et al.*, 2024), this study offers a clear methodological and conceptual advance. Its primary contribution lies in the integration of three monitoring campaigns conducted over a four-year period (2020–2024), which allows interannual hydrochemical variability and climate-related influences on groundwater quality in a semi-arid alluvial aquifer to be explicitly examined rather than inferred. In contrast to previous studies that employ the Water Quality Index mainly as a static classification tool, the present work embeds WQI within a process-based framework that combines hydrochemical facies analysis, ion-exchange diagnostics, and mineral saturation evaluation to identify the geochemical mechanisms governing water quality evolution. By systematically relating temporal changes in individual physicochemical parameters to both geogenic processes and WQI responses, the study provides new insight into the interplay between natural buffering capacity and emerging anthropogenic pressures in shallow aquifer systems. Focusing on the Bousselam Upstream River alluvial aquifer (an important yet poorly documented water resource in northern Algeria) this research addresses a critical regional knowledge gap and delivers transferable analytical and interpretative approaches applicable to groundwater assessment and management in semi-arid environments.

In north-eastern Algeria, the BUR serves as a vital tributary feeding the Ain Zada Dam, which supplies multiple communities in the Setif province. The river is increasingly impacted by domestic wastewater, agricultural runoff, industrial effluents, livestock operations, and treated discharges from the Setif wastewater treatment plant, highlighting the urgent need for comprehensive hydrochemical assessment.

Within the broader context of progressive water quality deterioration documented in semi-arid regions of the hight plain region, the hydrogeological configuration of the BUR basin represents a particularly revealing system in which regional-scale pressures are expressed through local geological and hydrodynamic controls. Groundwater circulation occurs within a structurally complex alluvial aquifer embedded in a heterogeneous assemblage of carbonate bedrock and Quaternary deposits, a configuration that exerts a first-order control on recharge processes, groundwater residence times, and the geochemical pathways governing solute acquisition. The predominance of permeable carbonate formations favors rapid infiltration and sustained water-rock interaction, while the overlying alluvial materials facilitate lateral exchanges between surface water and groundwater. This hydraulic openness, combined with the shallow depth of the aquifer, markedly increases its exposure to surface-derived fluxes associated with agricultural practices, urban expansion, and industrial activities. As a result, natural geochemical processes such as carbonate and evaporite dissolution, ion exchange, and salinity accumulation operate in concert with superimposed anthropogenic inputs, producing a hydrochemical signal that is both process-driven and pressure-responsive. Situating the Bousselam basin within the wider regional narrative of groundwater degradation therefore requires explicit consideration of how its geological architecture and hydrogeological functioning mediate the transfer, attenuation, or amplification of external stresses. This linkage provides a coherent framework for interpreting observed groundwater chemistry and underscores the basin's relevance as a representative model for understanding water quality dynamics in semi-arid alluvial systems under increasing climatic and human pressure.

This study adopts a multidisciplinary approach to evaluate the hydrogeochemical characteristics and water quality of the BUR through integrated field measurements, laboratory analyses, hydrochemical facies interpretation, and WQI computation within a GIS framework. The objectives are to (*i*) characterize the geological and hydrogeological context of the basin, (*ii*) identify the key physicochemical parameters influencing water quality, (*iii*) compute and spatially map WQI to evaluate domestic and irrigation suitability, and (*iv*) interpret relationships between individual water quality parameters and overall WQI results. Beyond informing local water management strategies, these findings offer transferable insights for sustainable groundwater assessment in semi-arid regions globally, where the combined pressures of climate variability and human activity pose comparable challenges.

STUDY AREA

The Wady Boussellam Valley, located in northeastern Algeria, constitutes a key hydrological system within the Setif region and serves as a critical source of surface and groundwater for domestic, agricultural, and industrial use (Fig. 1). The valley faces mounting environmental pressures due to rapid urban expansion, intensive land use, and the proliferation of industrial and agricultural activities, which collectively compromise its natural regulatory functions, including pollutant filtration and aquifer recharge. Agricultural practices, livestock rearing, and extractive industries such as mining and quarrying contribute both point- and diffuse-source pollution, driving progressive degradation of water quality.

Hydrologically, the Boussellam Upstream River (BUR) forms the primary drainage axis of the region. It originates at Ras Ain Boussellam, north of Farmatou, flowing ~159 km southwest to the Wady Soummam, with an annual regulated flow of ~38 million m³ (DRE, Setif). The basin, covering ~4,300 km², is fed by two principal tributaries; Wady Guessar along the southern Jebel Megress foothills (1,737 m) and Wady Ouricia on the massif's southern flank. The river traverses multiple settlements, including Bougaâ, Hammam Guergour, Wady Sebt, and Charchar, ultimately discharging into the Ain Zada Dam (125 million m³), which supplies nearly one million inhabitants across Setif, El Eulma, Ain Arnat, Bougaâ, Beni Oucine, and Bordj Bou Arreridj. Seasonal snowmelt from Jebel Megress and numerous perennial springs largely control the river's flow regime, which exhibits pronounced seasonal variability (peak February flows ~56 m³/s; low August flows ~1.1 m³/s). Morphometric characteristics include a basin area of 1,800 km², perimeter of 175 km, average slope of 2.71 m/km, and thalweg length of ~65 km.

Geologically, the basin lies within the Setifian high plains and is dominated (~70%) by highly permeable calcareous formations, favoring groundwater recharge. Quaternary deposits include lacustrine limestones and recent alluvium, while Mio-Pliocene sequences comprise fluvio-lacustrine sands, gravels, silts, and clays. The river corridor is bordered by Eocene Tellian formations, ranging

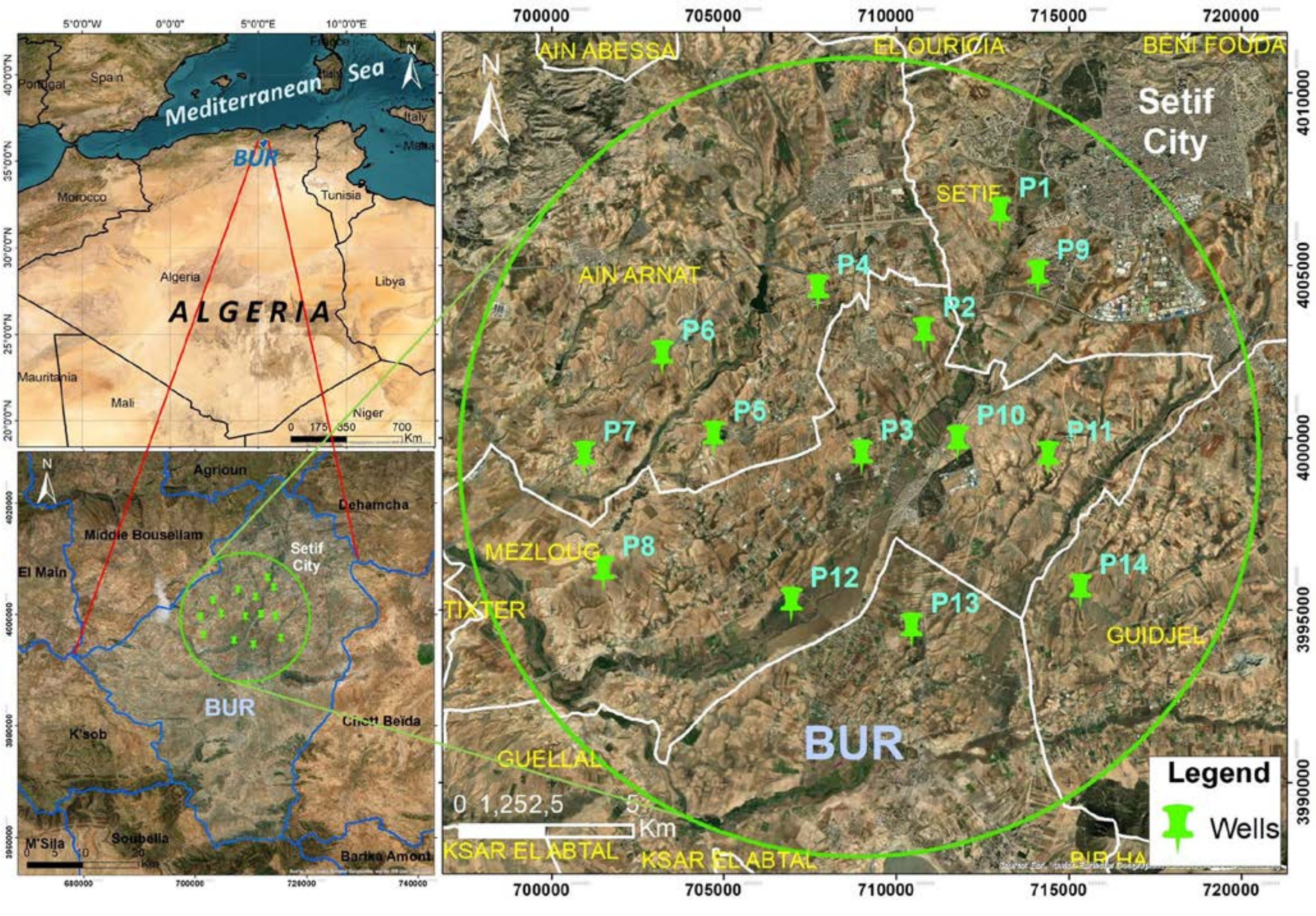

Fig. 1. Geographical location of the study area.

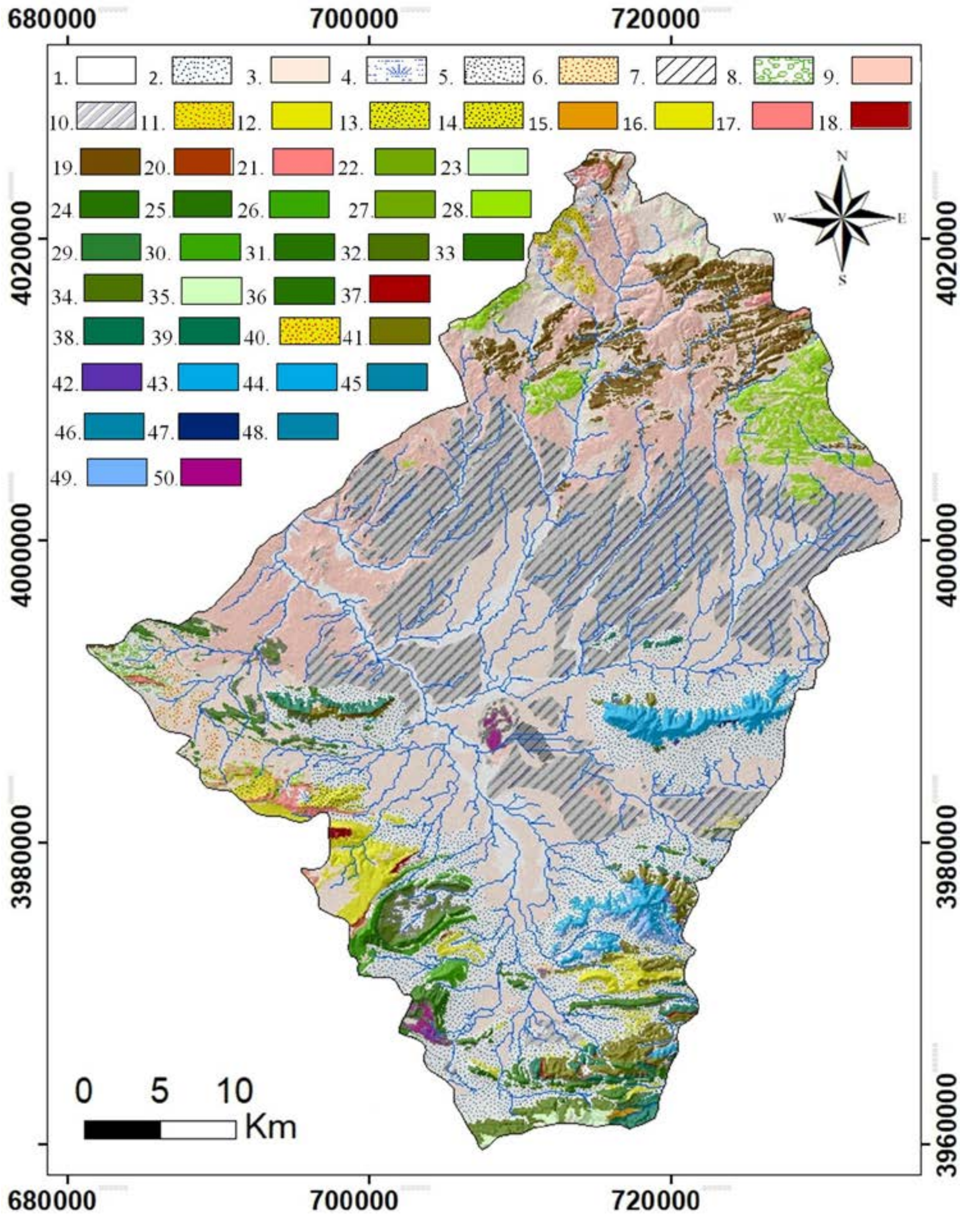

Fig. 2. Simplified geological map of BUR. 1 – recent alluvium, 2 – polygenic glacis deposits, 3 – undifferentiated Quaternary deposits, 4 – Quaternary scree, 5 – Quaternary dunes, 6 – Quaternary calcareous crust, 7 – sebkha deposits, 8 – topsoil and marly eluvium, 9 – Mio-Pliocene continental deposits, 10 – probable Villafranchian lacustrine-fluvial deposits, 11 – lower Miocene clay and sand, 12 – Miocene conglomerates and marls, 13 – lower Miocene marls, 14 – marine Miocene sandstones and marls, 15 – Oligocene conglomerates and sandstones, 16 – Eocene detrital limestones, 17 – middle–upper Eocene marls, 18 – upper Lutetian gypsiferous clay and limestones, 19 – Ypresian–lower Lutetian marly limestones, 20 – Ypresian–lower Lutetian phosphatic limestones, 21 – Palaeocene–lower Eocene marls, 22 – Maastrichtian–Danian marls and limestones, 23 – Maastrichtian–Palaeocene marls, 24 – upper Senonian marls and limestones, 25 – upper Senonian bioclastic limestones, 26 – upper Senonian marly limestones, 27 – Campanian–lower Maastrichtian marls, 28 – Campanian–Maastrichtian limestones, 29 – Santonian–Campanian marly limestones, 30 – Coniacian–Santonian marls and limestones; 31 – upper Coniacian–Santonian marls, 32 – Cenomanian–Turonian limestones and dolomites, 33 – Cenomanian–Turonian limestones, 34 – Vraconian–lower Cenomanian marls and limestones, 35 – Albian limestones and marls, 36 – upper Aptian–Albian clay and marls, 37 – Aptian marls, 38 – Aptian limestones and dolomites, 39 – upper Aptian limestones, 40 – coarse-grained sandstones, 41 – Barremian limestones and marls, 42 – Neocomian sandstones and marls, 43 – upper Jurassic limestones, 44 – upper Jurassic dolomites, 45 – middle Jurassic limestones, 46 – Jurassic–Cretaceous transitional limestones, 47 – lower Jurassic dolomites, 48 – upper Lias marls and limestones, 49 – Dogger marly limestones, 50 – exotic Triassic clay, gypsum, and dolomites.

from dark marls and clayey limestones to massive gray and white limestones, with lithological variations strongly influencing mineralization and water quality.

The lithostratigraphy of the study area is underlain by a thick continental sedimentary succession reflecting the combined influence of tectonic activity, sediment supply, and climatic variability from the Mesozoic through the Quaternary. Structurally, the plain occupies a transitional zone between the Tellian Atlas to the north and the Saharan Atlas and adjacent intracontinental basins to the south, promoting the deposition of detrital and chemical sediments sourced from uplifted Meso-Cenozoic terrains that form the deeper structural substratum (Savornin, 1920; Vila, 1980).

The overlying filling cover is dominated by Mio-Plio-Quaternary continental formations, which unconformably rest on older units and host the region's principal aquifers. These deposits are characterized by vertically and laterally heterogeneous sequences of lacustrine limestones, clay-rich intervals, sandy silts, and coarse alluvial conglomerates. This lithological variability records repeated shifts between fluvial, lacustrine, and floodplain environments, driven by fluctuating subsidence rates, hydrological regimes, and climatic conditions. Carbonate-rich lacustrine horizons indicate phases of reduced clastic input and enhanced chemical precipitation, whereas coarse alluvial facies reflect periods of intensified erosion and sediment transport from surrounding reliefs.

Quaternary alluvial and colluvial deposits further blanket much of the plain. These surficial sequences, comprising terrace gravels, active and abandoned channel fills, and fine-grained overbank sediments, document late Pleistocene to Holocene hydrological fluctuations. Their spatially extensive but texturally variable nature imposes strong controls on infiltration, hydraulic connectivity, and aquifer vulnerability.

Taken together, this lithostratigraphic architecture establishes a laterally extensive yet internally heterogeneous hydrostratigraphic framework, where groundwater recharge, storage, and flow are intimately linked to facies distribution and depositional history. The Wady Boussellam basin thus represents a complex socio-environmental system where geological, hydrological, and anthropogenic factors converge, rendering the watershed highly sensitive to degradation. Understanding its hydrogeological and geochemical characteristics is essential not only for local water resource management but also for informing sustainable development strategies in semi-arid regions globally, where similar pressures threaten water security and ecosystem integrity.

MATERIAL AND METHODS

Groundwater sampling and field measurements

Groundwater samples were collected from the Quaternary alluvial aquifer of the Oued Boussellam valley, the primary source of domestic and agricultural water in the region. Fourteen wells were selected to provide representative spatial coverage across the aquifer, with locations chosen based on hydrogeological features, proximity to potential recharge zones, and variations in land use. This approach aimed to capture the heterogeneity in aquifer properties while accounting for potential influences of surface layers, including clay-rich horizons, which can impede infiltration and locally modify water chemistry. To assess both seasonal and interannual variability, three monitoring campaigns were conducted in 2020, 2022, and 2024, yielding a total of forty-two groundwater samples.

Prior to sampling, each well was purged for 10–15 minutes to remove stagnant water from the casing and obtain samples representative of the aquifer rather than localized stagnant zones. Field parameters (temperature, pH, and electrical conductivity (EC)) were measured in situ using a calibrated multiparameter probe with a combined electrode system. Sampling was initiated only after stabilization of these parameters to ensure the collection of undisturbed groundwater, with precautions taken to minimize air exposure and prevent oxidation or degassing.Samples were collected in pre-cleaned high-density polyethylene bottles. For cation analyses, subsamples were filtered through 0.45 µm cellulose acetate membranes and acidified to pH <2 using ultrapure nitric acid; anion samples were stored unacidified. All samples were kept at 4°C and transported to the laboratory within 24 hours to preserve chemical integrity.

The sampling strategy, consisting of fourteen wells systematically distributed across the Boussellam alluvial aquifer and surveyed over three campaigns, was designed to capture the inherent spatial heterogeneity and hydrogeological complexity of the system. Well locations were selected to encompass key variations in lithology, recharge potential, and land-use influences, thereby representing both coarse alluvial deposits and finer clay-rich layers that modulate infiltration and local water chemistry. Conducting repeated campaigns over multiple years allows for the evaluation of seasonal and interannual hydrochemical fluctuations, including those driven by climatic variability and anthropogenic pressures. This approach ensures that the dataset reflects both the overall aquifer behavior and site-specific deviations, providing a scientifically robust foundation for interpreting groundwater dynamics, assessing water quality trends, and supporting evidence-based management strategies in a complex alluvial environment.

Laboratory analyses and quality control

Analyses followed APHA (2017) and ISO-standardized procedures. Calcium (Ca^{2+}) and magnesium (Mg^{2+}) were quantified via EDTA complexometric titration, chloride (Cl^-) by argentometric titration with $AgNO_3$, sodium (Na^+) and potassium (K^+) by flame photometry, and bicarbonate (HCO_3^-) and carbonate (CO_3^{2-}) by acid titration with HCl. Sulfate (SO_4^{2-}) and nitrate (NO_3^-) were determined spectrophotometrically. All measurements were performed in triplicate and expressed in milliequivalents per liter (meq/L), with quality control protocols applied to ensure accuracy and reproducibility.

Analytical reliability was assessed using the ionic balance error (IBE):

$$IBE = ((\Sigma cations - \Sigma anions) / (\Sigma cations + \Sigma anions)) \times 100\% \quad \text{Eq. 1}$$

where ∑cations and ∑anions represent the total concentrations of major cations and anions, respectively. Analytical results were considered acceptable when |IBE| ≤ ±8%.

Hydrogeochemical characterization

Groundwater hydrogeochemistry was interpreted using major ion concentrations to identify dominant water types, temporal evolution, and controlling geochemical processes. Hydrochemical facies were determined using Piper, Schoeller, Berkaloff, and Stiff diagrams generated with Diagrammes software (version 6.77). These graphical approaches facilitated comparison between sampling periods and supported classification of groundwater for domestic and irrigation uses.

Water hardness

Total groundwater hardness was calculated from Ca^{2+} and Mg^{2+} concentrations and expressed as hydrotimetric title in French degrees (°F), where 1°F corresponds to 10 mg/L $CaCO_3$. Carbonate and non-carbonate hardness were distinguished based on the origin of dissolved salts. Hardness classes followed WHO (1993) criteria, ranging from very soft (<7°F) to very hard (>40°F).

Ion exchange processes

Ion-exchange reactions between groundwater and aquifer materials were evaluated using the Base Exchange Index (IEB) (Schäffer and Dietz, 2023):

$$IEB = (rCl^- - (rNa^+ + rK^+)) / (rCl^-) \qquad \text{Eq. 2}$$

Positive IEB values indicate direct ion exchange, values close to zero indicate equilibrium conditions, and negative values reflect inverse ion exchange.

Mineral Saturation and Water Aggressiveness

Mineral saturation states were assessed using the saturation index (SI), also referred to as the Langelier Saturation Index:

$$SI = \log (PAI / Ks) \qquad \text{Eq. 3}$$

Saturation indices were calculated for carbonate minerals (calcite, dolomite, and aragonite) and sulfate minerals (gypsum and anhydrite) to evaluate dissolution–precipitation processes, groundwater aggressiveness, and scaling potential.

Water Quality Index (WQI)

Overall groundwater quality was evaluated using the Water Quality Index (WQI) method originally proposed by Horton (1965) and refined by Brown *et al.* (1970). Each parameter was assigned a relative weight (W_i):

$$Wi = k/Si \qquad \text{Eq. 4}$$

where S_i is the permissible standard value according to Algerian regulations (Decree of March 23, 2011), and k is a proportionality constant defined as:

$$k = 1/(\sum_{n}^{i=1} (1/Si)) \qquad \text{Eq. 5}$$

The quality rating for each parameter (Q_i) was calculated as:

$$Qi = (Ci/Si)\times 100 \qquad \text{Eq. 6}$$

where Ci is the measured concentration. The overall WQI was then computed as:

$$WQI = \frac{\sum_{i=1}^{n} W_i Q_i}{W_i} \qquad \text{Eq. 7}$$

Groundwater quality was classified into five categories ranging from excellent to unsuitable for use. WQI values were calculated for each sampling campaign, and spatial distribution maps were produced using Microsoft Excel and ArcGIS 10.8.

Irrigation water suitability

Groundwater suitability for irrigation was assessed using salinity and sodicity indicators, including the Sodium Adsorption Ratio (SAR):

$$SAR = \frac{Na^+}{\sqrt{(Ca^{2+} + Mg^{2+})/2}} \qquad \text{Eq. 8}$$

Irrigation water was classified into sodicity hazard classes (S1–S4) following Durand (1982). Sodium percentage was calculated as:

$$\%Na = \frac{Na}{Ca^{2+} + Mg^{2+} + Na^+ + K^+} \times 100 \qquad \text{Eq. 9}$$

The combined interpretation of SAR, EC, sodium percentage, and Wilcox and Richards classifications enabled evaluation of potential risks related to soil salinization, sodification, and structural degradation under irrigation practices.

RESULTS

Physicochemical data obtained from the three monitoring campaigns (2020, 2022, and 2024; Tables 1 and 2) provide a robust basis for evaluating the temporal evolution of groundwater quality in the Boussellam alluvial aquifer (BUR). Overall, groundwater chemistry remains broadly stable over the four-year period, with moderate variations reflecting the combined effects of intrinsic hydrogeochemical controls and evolving anthropogenic pressures.

Groundwater pH values range from 6.8 to 7.4, indicating neutral to slightly alkaline conditions typical of carbonate-

Table 1. Physicochemical analyses of the three campaigns (2020, 2022, and 2024).

Nom	Ca^{2+} (mg/l)	Mg^{2+} (mg/l)	Na^{+} (mg/l)	Cl^{-} (mg/l)	HCO^{3-} (mg/l)	SO_4^{-2} (mg/l)	NO^{3-} (mg/l)	C E (µs/cm)	T (°C)	pH
2020 Campaign										
P1	120	60	90	165	270	195	21	1245	17.9	7.1
P2	135	49	85	155	195	240	18	1305	17.5	7.2
P3	125	68	105	180.1	270	205.45	19.45	1466	16.3	6.9
P4	125	65	70	168	227	218	19.5	1157	16.4	7.2
P5	120	75	78.6	155	203.1	285	19.3	1433	17.1	7
P6	121.5	82	68	155.8	247	179.1	18.2	1415	15.9	7.3
P7	145.6	76	98	216	328.9	228.9	25.1	1613	15.6	7
P8	162.7	63	89	241.3	248	239.4	23.89	1591	16.2	7.2
P9	110	45	78.5	161	201.85	217.5	20.5	1222	16.8	7.4
P10	150	70	100.5	155.8	300.5	226	21.45	1406	17.5	6.9
P11	118	65	100.5	150	155	245	16	1273	16.3	7.4
P12	160	65	110.8	172.5	330.5	252.4	21.25	1560	17.4	7.2
P13	136	72	59	162.4	298	225.98	22.43	1369	16.2	7.2
P14	150	85	168	192	300.5	285	19.45	1459	15.4	7.4
2022 Campaign										
P1	101	37	77	158	305	200	19	1255	17.9	7.1
P2	135	44	93	149	218	247	23	1300	17.5	7.2
P3	111	68	102	185	295	219	21.5	1445	16.3	6.9
P4	83	51	83	167	230.2	118.57	17.85	1200	16.4	7.2
P5	95	70	78	160	230	302.5	21.05	1452	17.1	7
P6	112	81	68.5	165	246	179	19.5	1420	15.9	7.3
P7	149	75	101	222	228	221	24.25	1632	15.6	7
P8	164	62.35	98.9	244	244.62	237	23.01	1600	16.2	7.2
P9	102	41	75.9	161.25	198.5	221.85	21.95	1235	16.8	7.4
P10	99	66	99.6	159.5	298.65	232.5	23.38	1410	17.5	6.9
P11	103	38	99.65	155	158	258.5	18.95	1280	16.3	7.4
P12	148.26	62.32	104.52	179.25	335	256	21	1562	17.4	7.2
P13	139.28	71.24	57.98	157.89	294.25	225.36	19.24	1375	16.2	7.2
P14	135	88.25	84.27	118	298	295.86	19.85	1460	15.4	7.4
2024 Campaign										
P1	100	38	76	160	302	205	22	1244	17.8	7
P2	140	45	92	155	202	245	23	1330	17	7.1
P3	115	69	104	185	300	220	21	1463	16.1	6.8
P4	85	51	85	170	230	120	19.5	1154	16.4	7.1
P5	102	73	80	160	230	305	23.5	1431	17	7.1
P6	120	85	70	159	245	178	19.5	1416	16	7.3
P7	150	75	100	220	330	230	25	1612	15.4	7.1
P8	165	64	100	245	250	240	23	1590	16	7.1
P9	101	42	75	162	200	220	22.6	1219	16.5	7.2
P10	121	66	100	160	300	230	25.5	1405	17.5	6.8
P11	105	39	100	155	160	265	21.5	1270	16.2	7.3
P12	160	63	101	180	340	260	22	1558	17.2	7.1
P13	140	72	60	158	300	227	23	1365	16.1	7.1
P14	150	87	82	110	310	298	21	1460	15.3	7.3

dominated aquifers. The limited temporal variability of pH points to an effective buffering system governed by carbonate dissolution and the bicarbonate-CO_2 equilibrium. Measured groundwater temperatures (15.3–17.9°C) are consistent with shallow alluvial settings and reflect seasonal climatic influences rather than deep geothermal control.

Electrical conductivity (EC) values vary between 1154 and 1632 µS/cm, indicating moderate to high mineralization. The highest EC values recorded in 2022 coincide with a period of reduced recharge, suggesting enhanced evapoconcentration during drier conditions. Major ion chemistry is dominated by calcium (83–165 mg/L), magnesium (37–88 mg/L), and bicarbonate (155–340 mg/L), confirming the central role of carbonate weathering (calcite and dolomite) in controlling groundwater composition. Sulfate concentrations (118–302 mg/L) are consistently elevated, with higher values in 2022 and 2024, reflecting sustained gypsum dissolution. Sodium (57–104 mg/L) and chloride (110–245 mg/L) show a slight but coherent increase toward 2024, while nitrate concentrations

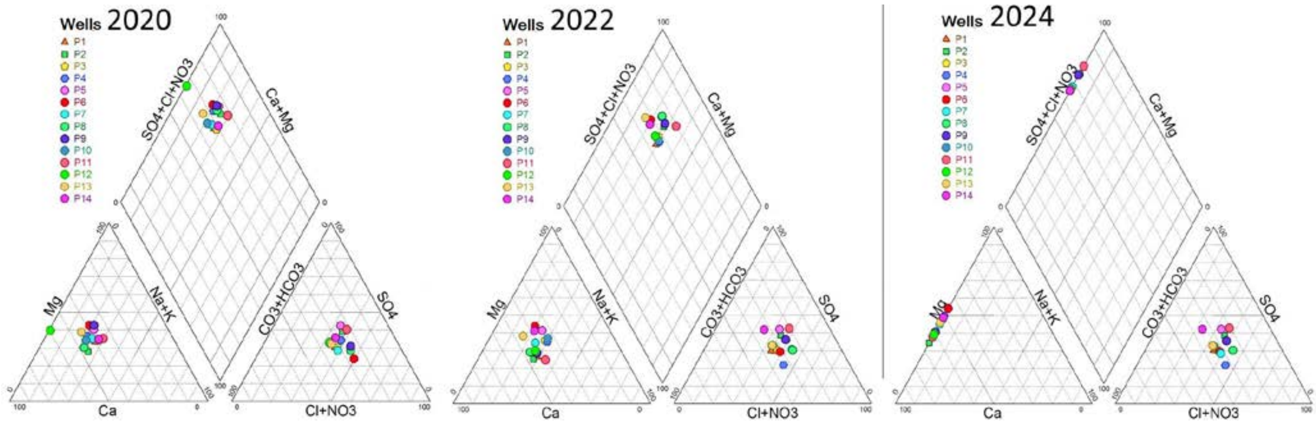

Fig. 3. Evolution of groundwater chemical facies in 2020, 2022 and 2024 presented on Piper Diagrams.

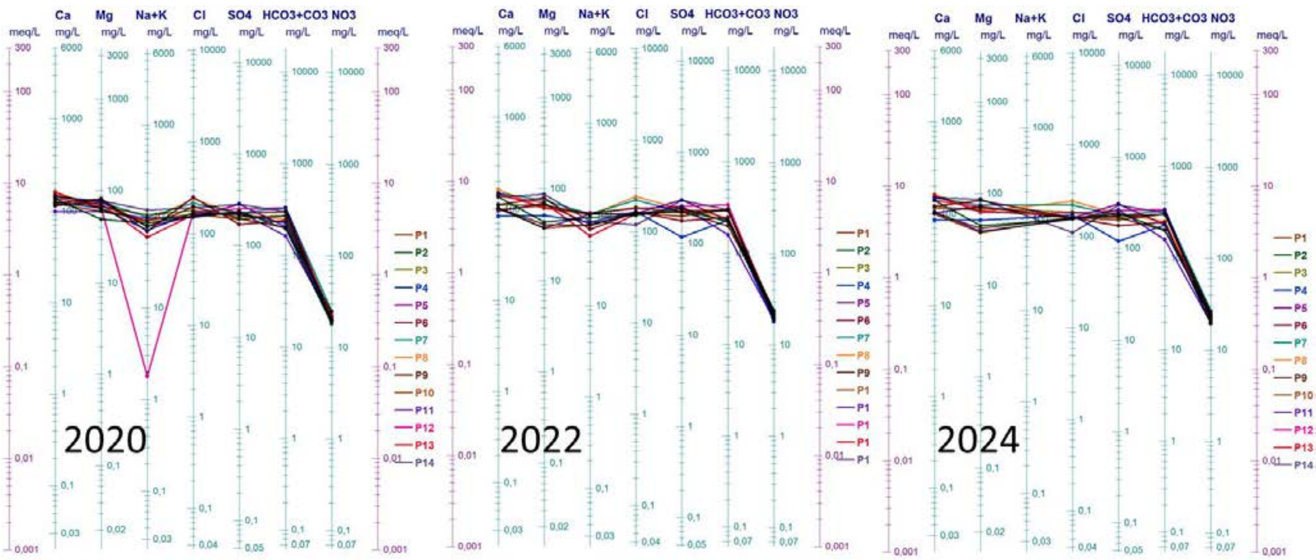

Fig. 4. Changes in major cations and anions in groundwater samples between 2020, 2022 and 2024.

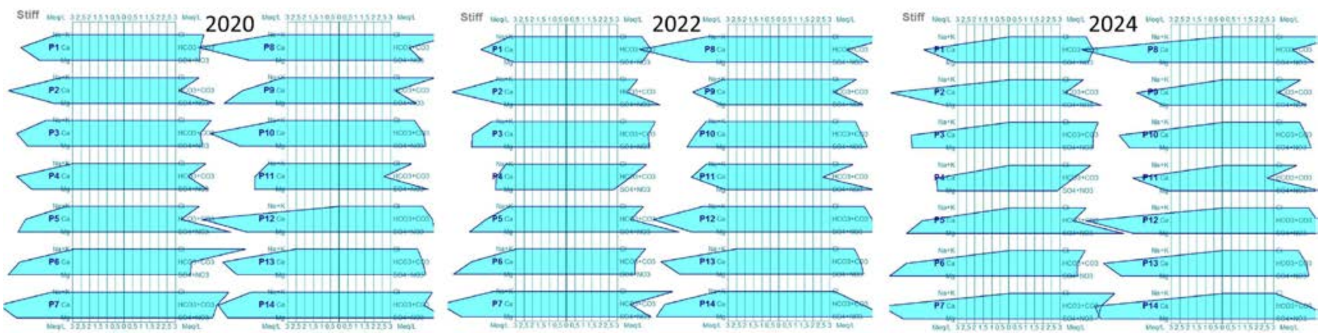

Fig. 5. Temporal variation of groundwater hydrochemical facies based on Stiff diagrams (2020–2024).

(16–25.5 mg/L) remain below WHO drinking-water limits but display a gradual upward trend, indicative of diffuse anthropogenic inputs.

Hydrochemical facies analysis using Piper, Berkaloff, and Stiff diagrams (Figs. 3–5) reveals a predominance of sulfate-chloride-calcium-magnesium water types. In 2020, four principal facies were identified: calcium chloride, magnesium chloride, calcium sulfate, and magnesium sulfate. Most monitoring points exhibit stable facies over time, underscoring the persistence of the governing geochemical processes. However, localized deviations were observed at wells P1, P4, and P9, including a partial shift toward bicarbonate-enriched waters at P1, likely reflecting episodic recharge or dilution events (Tables 3 and 4).

Total hardness values generally range between 40 and 73°F, classifying the groundwater as hard to very hard

Table 2. Descriptive statistics of the physicochemical parameters recorded during the three monitoring campaigns conducted in 2022, 2023, and 2024.

Campaign		T°C	pH	C.E	Ca^{2+}	Mg^{2+}	Na^{+}	Cl^{-}	HCO_3^{-}	SO_4^{2-}	NO_3^{-}
2020	Min	15.4	6.9	1157	118	49	68	150	155	179.1	16
	Max	17.9	7.4	1613	162.7	85	168	241.3	330.5	285	23.89
	Mean.	16.607	7.171	1393.86	134.2	67.14	92.92	173.6	255.38	231.62	20.39
	E.t	0.77	0.172	140.598	16.85	11.14	26.37	26.36	53.790	29.97	2.391
2022	Min	15.4	6.9	1200	83	37	57.98	118	158	118.57	19
	Max	17.9	7.4	1632	148.3	88.25	104.52	244	335	302.5	24.25
	Mean.	16.61	7.17	1401.86	113.97	61.08	87.38	170.06	255.65	229.5	20.96
	E.t	0.77	0.17	136.47	22.96	16.39	14.50	30.97	49.549	46.10	1.965
2024	Min	15.3	6.8	1154	85	38	60	110	160	120	19.5
	Max	17.8	7.3	1154	165	87	104	245	340	298	25.5
	Mean.	16.464	7.1	1361.35	125.28	62.07	87.5	169.9	264.21	231.6	22.29
	E.t	0.7458	0.156	138.71	25.42	16.47	13.98	31.77	54.915	46.65	1.763

Table 3. Evolution of Groundwater Hydrochemical Facies Based on Major Ion Dominance (2020–2024).

Sample	Dominant ions (Formula)	Hydrochemical facies
Facies 2020		
P1	Cl>HCO_3>Ca>Mg	Calcium-magnesium chloride-bicarbonate type
P2	SO_4>Ca	Calcium sulfate type
P3	Cl>Ca>Mg	Calcium-magnesium chloride type
P4	SO_4>Cl>Ca>Mg	Magnesium-calcium sulfate-chloride type
P5	SO_4>Cl>Mg>Ca	Magnesium-calcium sulfate-chloride type
P6	Cl>Mg>Ca	Magnesium-calcium chloride type
P7	Cl>HCO_3>Ca>Mg	Calcium-magnesium chloride-bicarbonate type
P8	Cl>Ca	Calcium chloride type
P9	Cl>SO_4>Mg>Ca	Magnesium-calcium chloride-sulfate type
P10	SO_4>HCO_3>Ca>Mg	Calcium-magnesium sulfate-bicarbonate type
P11	SO_4>Cl>Ca>Mg	Calcium-magnesium sulfate-chloride type
P12	SO_4>HCO_3>Ca>Mg	Calcium-magnesium sulfate-bicarbonate type
P13	SO_4>HCO_3>Ca>Mg	Calcium-magnesium sulfate-bicarbonate type
P14	SO_4>Cl>Ca>Mg	Calcium-magnesium sulfate-chloride type
Facies 2022		
P1	HCO_3>Ca	Calcium bicarbonate type
P2	SO_4>Cl>Ca	Calcium sulfate-chloride type
P3	Cl>Ca>Mg	Calcium-magnesium chloride type
P4	Cl>Mg>Ca	Calcium-magnesium chloride type
P5	SO_4>Cl>Mg>Ca	Magnesium-calcium sulfate-chloride type
P6	Cl>Mg>Ca	Magnesium-calcium chloride type
P7	Cl>SO_4>Ca>Mg	Calcium-magnesium chloride-sulfate type
P8	Cl>SO_4>Ca	Calcium chloride-sulfate type

Sample	Dominant ions (Formula)	Hydrochemical facies
Facies 2020		
P9	SO_4>Cl>Ca	Calcium sulfate-chloride type
P10	SO_4>Mg	Magnesium sulfate type
P11	SO_4>Cl>Ca>Na	Calcium-sodium sulfate-chloride type
P12	SO_4>HCO_3>Ca	Calcium sulfate-bicarbonate type
P13	SO_4>HCO_3>Ca>Mg	Calcium-magnesium sulfate-bicarbonate type
P14	SO_4>HCO_3>Mg>Ca	Magnesium-calcium sulfate-bicarbonate type
Facies 2024		
P1	HCO_3>Ca>Mg	Calcium-magnesium bicarbonate type
P2	SO_4>Cl>Ca	Calcium sulfate-chloride type
P3	Cl>Ca>Mg	Calcium-magnesium chloride type
P4	Cl>Ca>Mg	Calcium-magnesium chloride type
P5	SO_4>Cl>Mg>Ca	Magnesium-calcium sulfate-chloride type
P6	Cl>Mg>Ca	Magnesium-calcium chloride type
P7	Cl>Ca>Mg	Calcium-magnesium chloride type
P8	Cl>SO_4>Ca>Mg	Calcium-magnesium chloride-sulfate type
P9	SO_4>Cl>Ca>Mg	Calcium-magnesium sulfate-chloride type
P10	SO_4>Ca>Mg	Calcium-magnesium sulfate type
P11	SO_4>Cl>Ca>Mg	Calcium-magnesium sulfate-chloride type
P12	SO_4>HCO_3>Ca>Mg	Calcium-magnesium sulfate-bicarbonate type
P13	SO_4>HCO_3>Ca>Mg	Calcium-magnesium sulfate-bicarbonate type
P14	SO_4>HCO_3>Ca>Mg	Calcium-magnesium sulfate type

Table 4. Temporal Evolution of Groundwater Hydrochemical Facies Formulas (2020–2024).

Sample	Hydrochemical facies	Formula (2020)	Formula (2022)	Formula (2024)
P1	Calcium-magnesium chloride-bicarbonate → Calcium bicarbonate → Calcium-magnesium bicarbonate	Cl>HCO_3>Ca>Mg	HCO_3>Ca	HCO_3>Ca>Mg
P2	Calcium sulfate → Calcium sulfate-chloride → Calcium sulfate-chloride	SO_4>Ca	SO_4>Cl>Ca	SO_4>Cl>Ca
P3	Calcium-magnesium chloride (stable)	Cl>Ca>Mg	Cl>Ca>Mg	Cl>Ca>Mg
P4	Magnesium-calcium sulfate-chloride → Calcium-magnesium chloride	SO_4>Cl>Ca>Mg	Cl>Mg>Ca	Cl>Ca>Mg
P5	Magnesium-calcium sulfate-chloride (stable)	SO_4>Cl>Mg>Ca	SO_4>Cl>Mg>Ca	SO_4>Cl>Mg>Ca
P6	Magnesium-calcium chloride (stable)	Cl>Mg>Ca	Cl>Mg>Ca	Cl>Mg>Ca
P7	Calcium-magnesium chloride-bicarbonate → Calcium-magnesium chloride-sulfate → Calcium-magnesium chloride	Cl>HCO_3>Ca>Mg	Cl>SO_4>Ca>Mg	Cl>Ca>Mg
P8	Calcium chloride → Calcium chloride-sulfate → Calcium-magnesium chloride-sulfate	Cl>Ca	Cl>SO_4>Ca	Cl>SO_4>Ca>Mg
P9	Magnesium-calcium chloride-sulfate → Calcium sulfate-chloride → Calcium-magnesium sulfate-chloride	Cl>SO_4>Mg>Ca	SO_4>Cl>Ca	SO_4>Cl>Ca>Mg
P10	Calcium-magnesium sulfate-bicarbonate → Magnesium sulfate → Calcium-magnesium sulfate	SO_4>HCO_3>Ca>Mg	SO_4>Mg	SO_4>Ca>Mg
P11	Calcium-magnesium sulfate-chloride → Calcium-sodium sulfate-chloride → Calcium-magnesium sulfate-chloride	SO_4>Cl>Ca>Mg	SO_4>Cl>Ca>Na	SO_4>Cl>Ca>Mg
P12	Calcium-magnesium sulfate-bicarbonate (slightly variable)	SO_4>HCO_3>Ca>Mg	SO_4>HCO_3>Ca	SO_4>HCO_3>Ca>Mg
P13	Calcium-magnesium sulfate-bicarbonate (stable)	SO_4>HCO_3>Ca>Mg	SO_4>HCO_3>Ca>Mg	SO_4>HCO_3>Ca>Mg
P14	Calcium-magnesium sulfate-chloride → Magnesium-calcium sulfate-bicarbonate → Calcium-magnesium sulfate-bicarbonate	SO_4>Cl>Ca>Mg	SO_4>HCO_3>Mg>Ca	SO_4>HCO_3>Ca>Mg

Table 5. Volution of Groundwater Total Hardness (TH) and Ionic Equilibrium Balance (IEB) from 2020 to 2024.

Sample	2020		2022		2024	
	TH	IEB	TH	IEB	TH	IEB
P1	55	0.159	40	0.248	41	0.13
P2	54	0.154	52	0.037	53	0.125
P3	59	0.101	56	0.15	57	0.11
P4	58	0.357	42	0.234	42	0.31
P5	60	0.218	53	0.248	55	0.25
P6	64	0.581	61	0.360	65	0.54
P7	68	0.3	68	0.298	68	0.27
P8	67	0.341	67	0.375	67	0.321
P9	62	0.402	42	0.274	42	0.41
P10	66	0.174	52	0.037	57	0.168
P11	49	0.019	41	0.009	42	0.018
P12	67	0.984	63	0.101	66	0.89
P13	64	0.44	64	0.434	65	0.42
P14	68	0.049	70	-0.101	73	0.039

(Table 5). Persistently high hardness at wells P7, P8, P13, and P14 contrasts with the temporary reduction observed at P1, P4, and P9 in 2022, before returning to previous levels in 2024. These variations remain secondary to the overall hydrochemical framework dominated by carbonate and sulfate mineral dissolution.

Base Exchange Index results indicate a predominance of direct cation exchange throughout the monitoring period, with groundwater preferentially enriched in Ca^{2+} and Mg^{2+} relative to Na^+ and K^+, except at well P14 in 2022. Saturation index calculations (Table 6; Figs. 6a–c) show systematic undersaturation with respect to gypsum and anhydrite, confirming their ongoing dissolution, whereas calcite and dolomite display variable saturation states, reflecting spatial and temporal heterogeneity in dissolution-precipitation equilibria.

Water Quality Index (WQI) results (Tables 8, 9 and 10) reveal marked temporal dynamics. In 2020, more than half of the wells (8 out of 14) were classified as having good water quality. A deterioration was observed in 2022, when groundwater quality was generally suitable for agricultural and industrial uses. By 2024, a clear improvement is evident, with 12 wells showing enhanced WQI values, suggesting partial recovery of groundwater quality. Irrigation suitability assessment based on SAR and Wilcox classifications places most samples within the S1C3 category on the Riverside diagram (Table 11), indicating low sodium hazard but high salinity risk, which may constrain long-term agricultural use without appropriate salinity management practices (Durand, 1982).

DISCUSSION

The hydrochemical functioning of the Boussellam alluvial aquifer is characteristic of groundwater systems developed under semi-arid to Mediterranean climatic conditions, where water-rock interaction exerts a dominant control on chemical composition. The persistence of slightly alkaline pH, consistently high hardness, and the prevalence of sulfate-chloride-calcium-magnesium facies collectively indicate prolonged circulation of groundwater within carbonate- and evaporite-rich lithologies. These features reflect a mature geochemical system in which mineral dissolution processes, particularly involving calcite, dolomite, gypsum, and halite, largely govern groundwater chemistry. The predominance of direct cation ex-

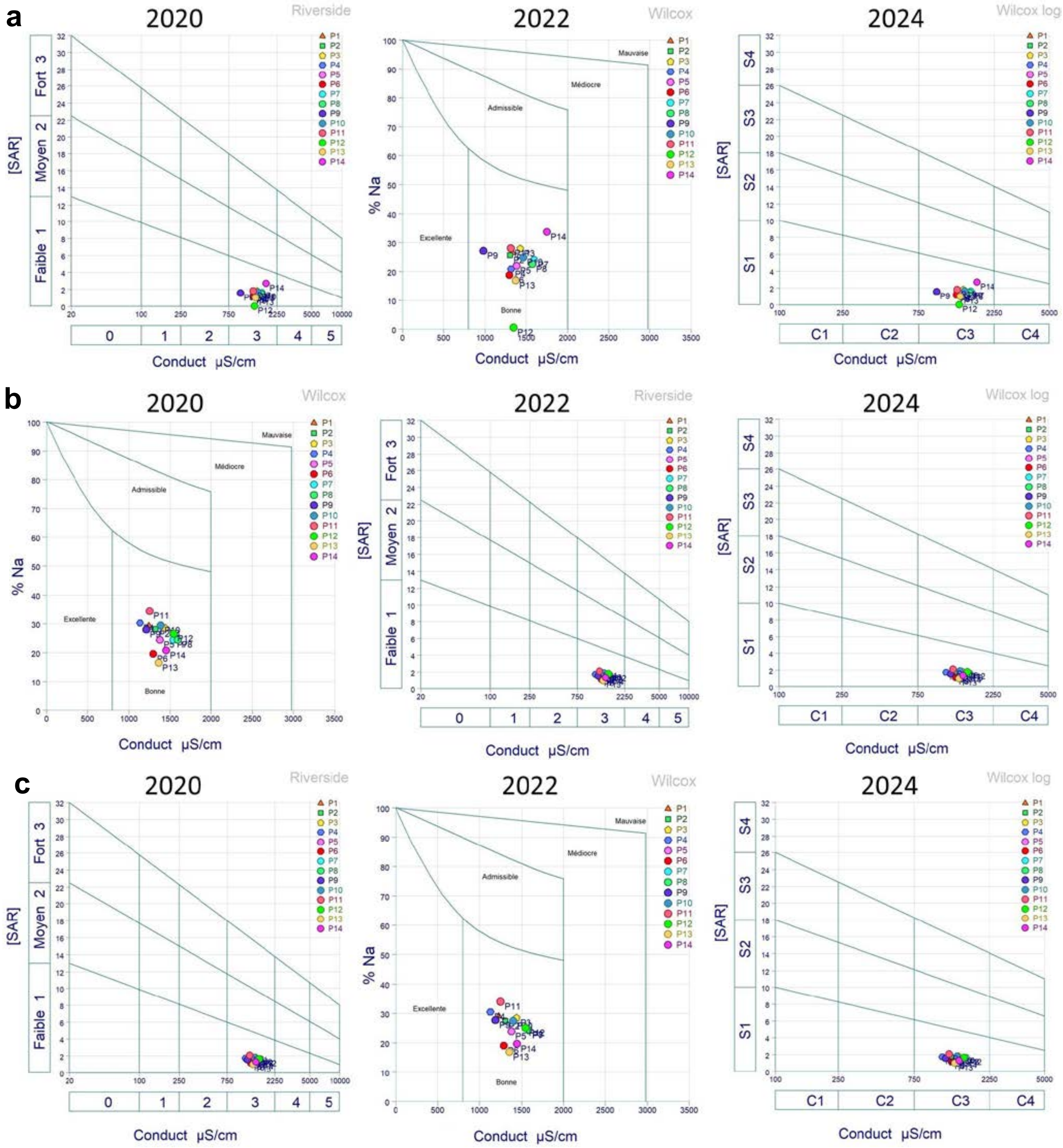

Fig. 6. a, b, c – Evolution of irrigation water quality from 2020 to 2024 based on Wilcox and Riverside diagram and Wilox log for 2020, 2022 and 2024.

change, as evidenced by positive Base Exchange Index values, further supports sustained interaction between groundwater and clay-bearing sediments, a behavior commonly observed in well-developed alluvial aquifers with long residence times.

Superimposed on this overall geochemical stability, temporal variations in electrical conductivity and major ion concentrations reveal the sensitivity of the aquifer to hydroclimatic forcing. The pronounced increase in mineralization during the 2022 campaign is consistent with periods of reduced recharge and enhanced evapoconcentration under dry conditions. Similar hydrochemical responses to climatic variability have been widely documented in semi-arid alluvial systems across North Africa, southern Europe, and the Middle East, where episodic recharge limits dilution and promotes solute accumulation. Nevertheless, the absence of major shifts in dominant ion assemblages suggests that the aquifer remains effectively buffered by carbonate equilibrium reactions, which moderate short-term chemical perturbations.

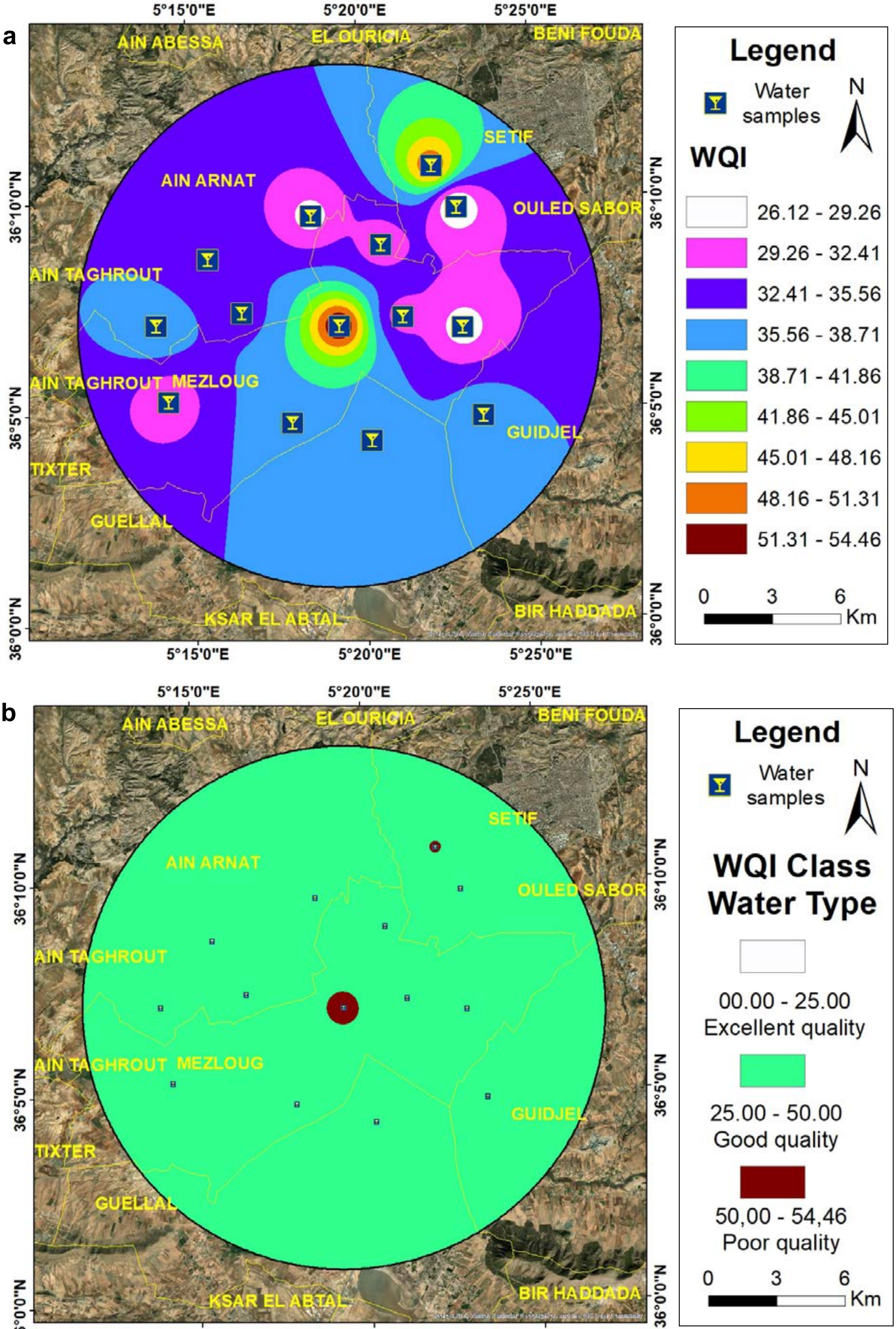

Fig. 7. a – Spatial distribution map of IWQ (Irrigation Water Quality). b – Groundwater quality map of the study area.

Table 6. Saturation indices of calcite, aragonite, dolomite, gypsum, and anhydrite for groundwater samples (2020–2024).

Wells	Calcite	Aragonite	Dolomite	Gypsum	Anhydrite
2020					
P1	-0.01	-0.16	0.02	-1.03	-1.25
P2	-0.10	-0.25	-0.29	-0.89	-1.11
P3	0.00	-0.15	0.08	-1.00	-1.22
P4	-0.07	-0.22	-0.08	-0.97	-1.19
P5	-0.17	-0.31	-0.16	-0.89	-1.11
P6	-0.07	-0.21	0.04	-1.10	-1.32
P7	0.13	-0.01	0.34	-0.90	-1.12
P8	0.06	-0.08	0.07	-0.88	-1.10
P9	-0.17	-0.32	-0.14	-0.89	-1.27
P10	0.11	-0.03	0.25	-1.03	-1.11
P11	-0.32	-0.47	-0.50	-0.81	-1.25
P12	0.19	0.04	0.34	-0.81	-1.03
P13	0.07	-0.07	0.22	-0.92	-1.14
P14	0.08	-0.07	0.25	-0.83	-1.05
2022					
P1	-0.02	-0.16	-0.12	-1.07	-1.29
P2	-0.06	-0.20	-0.25	-0.88	-1.10
P3	-0.02	-0.16	0.11	-1.02	-1.24
P4	-0.02	-0.36	-0.29	-1.37	-1.59
P5	-0.19	-0.33	-0.16	-0.95	-1.17
P6	-0.09	-0.23	0.04	-1.10	-1.32
P7	-0.01	-0.16	0.03	-0.90	-1.13
P8	0.06	-0.09	0.05	-0.84	-1.06
P9	-0.20	-0.35	-0.45	-1.03	-1.25
P10	-0.06	-0.20	0.06	-1.04	-1.26
P11	-0.30	-0.44	-0.68	-0.96	-1.18
P12	0.15	0.01	0.28	-0.84	-1.06
P13	0.08	-0.07	0.22	-0.91	-1.13
P14	0.06	-0.09	0.28	-0.82	-1.04
2024					
P1	-0.02	-0.16	-0.11	-1.06	-1.28
P2	-0.06	-0.21	-0.27	-0.85	-1.07
P3	0.02	-0.13	0.16	-0.99	-1.21
P4	-0.02	-0.34	-0.26	-1.34	-1.57
P5	-0.16	-0.30	-0.10	-0.91	-1.13
P6	-0.05	-0.20	0.10	-1.07	-1.29
P7	0.16	0.01	0.36	-0.88	-1.10
P8	0.08	-0.07	0.10	-0.82	-1.04
P9	-0.19	-0.34	-0.42	-1.02	-1.24
P10	0.04	-0.11	0.16	-0.95	-1.17
P11	-0.28	-0.42	-0.63	-0.93	-1.15
P12	0.20	0.05	0.35	-0.79	-1.01
P13	0.09	-0.05	0.25	-0.90	-1.12
P14	0.13	-0.02	0.37	-0.77	-0.99

The progressive enrichment in sodium, chloride, and nitrate observed toward 2024, while still below international drinking-water standards, points to diffuse and cumulative anthropogenic inputs linked primarily to agricultural practices and domestic wastewater infiltration. Such delayed responses are typical of shallow alluvial aquifers, where contaminants migrate slowly through the unsaturated zone before reaching the groundwater. Comparable trends have been reported in intensively cultivated plains of the Mediterranean basin, the Indo-Gangetic Plain, and parts of the Americas, underscoring the vulnerability of these systems to long-term land-use pressures. Importantly, the detected increases constitute early indicators of groundwater quality degradation, highlighting the value of sustained monitoring programs capable of capturing gradual changes that may otherwise remain undetected until regulatory thresholds are exceeded.

Hydrochemical facies analysis further illustrates the coexistence of regional stability and localized variability within the aquifer. While sulfate-chloride facies dominate across most wells throughout the monitoring period, isolated shifts toward bicarbonate-rich compositions suggest episodic recharge or dilution processes along preferential flow paths. This spatial heterogeneity reflects differences in residence time, hydraulic connectivity, and recharge intensity, and is a recurrent feature of extensive alluvial systems. Such localized departures from the dominant facies underscore the importance of site-specific hydrogeological conditions in shaping groundwater chemistry, even within aquifers exhibiting overall geochemical coherence.

The observed alternation between undersaturation and oversaturation with respect to carbonate minerals reveals a dual geochemical behavior with direct implications for groundwater exploitation and infrastructure durability. Waters undersaturated in calcite and dolomite retain an aggressive character, favoring continued mineral dissolution and potential corrosion of metallic installations, whereas oversaturated waters promote carbonate precipitation, leading to scaling and clogging of wells and distribution networks. This duality, frequently reported in aquifers hosted in mixed carbonate-evaporite sequences, represents a persistent operational challenge in semi-arid regions and underscores the need for tailored management strategies that account for spatial and temporal variations in water aggressiveness and scaling potential.

From a water-use perspective, the combination of high hardness and moderate to elevated salinity imposes constraints analogous to those encountered in many semi-arid agricultural regions worldwide. The classification of most samples within the S1C3 irrigation category indicates that sodium-related soil degradation risks remain limited, whereas salinity poses a more significant threat to soil structure and crop productivity. Without adequate drainage, leaching, and soil management practices, long-term irrigation with such water may lead to progressive soil salinization, with direct consequences for agricultural sustainability and food security in water-scarce environments.

Table 7. Classification and possible water use according to the WQI (Aher *et al.*, 2016).

WQI class	Water type	Usage
0–25	Excellent quality	Drinking water, irrigation, and industry
25–50	Good quality	Drinking water, irrigation, and industry
50–75	Poor quality	Irrigation and industry
75–100	Very poor quality	Irrigation
>100	Unsuitable water	Appropriate treatment required before use

Table 8. WQI for the P1 well.

Parameters	Norm (Si)	1/Si		$W_i = k/S_i$	Qi = Ci/Si × 100	Wi × qi	WQI = qi*wi/Wi
C.E	2800	0,00036	$k = \frac{1}{\sum_{i=1}^{n}(1/Si)}$ = 0.1313515	0.0000496	44.46	0.0022	0.00244
Ca^{2+}	200	0.005		0.000656	60	0.0393	0.0435
Mg^{2+}	150	0.0066		0.000875	40	0.035	0.0388
Na^{+}	200	0.005		0.000656	45	0.0295	0.0327
Cl^{-}	500	0.002		0.000262	33	0.008646	0.00958
HCO_{3-}	400	0.0025		0.000328	67	0.02197	0.0242
SO_4^{2-}	400	0.0025		0.000328	48	0.01574	0.0174
NO_3^{-}	50	0.02		0.00262	42	0.1104	0.122
NO_2	0.2	5		0.65675	50	32.8375	36.422
PO_4	0.4	2.5		0.328378	20	6.56756	7.284
		7.54146		Wi = 0.9015746	5.154 ×100 = 515.4 = Q1		WQI = 43.99

Table 9. Groundwater Quality Indices in the UBW, 2022–2024.

WQI	P1	P2	P3	P4	P5	P6	P7	P8	P9	P10	P11	P12	P13	P14
2020	43.99	82.33	37.43	63.93	71.22	43.5	57.31	54.64	183.35	33.84	30.91	38.24	32.73	43.8
2022	21.16	30.51	35.6	19.71	33.05	31.22	34.30	36.55	26.04	52.3	27.01	37	34.38	37.11
2024	50.54	30.60	54.46	28.22	34.48	32.33	38.26	30.06	26.12	31.06	27.72	37.66	36	37.58

Table 10. Groundwater Quality Indices in the UBW, 2022-2024.

WQI class	2020	2022	2024	Water quality and use
0–25		P1, P4		Excellent quality: Suitable for drinking, irrigation, and industrial use
25–50	P1, P3, P6, P10, P11, P12, P13, P14		P2, P4, P5, P6, P7, P8, P9, P10, P11, P12, P13, P14	Good quality: Suitable for drinking, irrigation, and industrial use
50–75	P4, P5, P7, P8	P2, P3, P5, P6, P7, P8, P9, P10, P11, P12, P13, P14	P1, P3	Poor quality: Suitable for irrigation and industrial use
75–100	P2			Very poor quality: Suitable for irrigation only
>100	P9			Unsuitable water: Requires appropriate treatment before use

Table 11. Classification of Water Quality Based on Soil Alkalinization Hazard (SAR).

Class name	Class range (SAR)	Description and uses
C1	0 < SAR ≤ 10 low sodium level	Water suitable for irrigating almost all types of soils. The alkalinization hazard is low, although certain sodium-sensitive crops may be slightly affected.
C2	10 < SAR ≤ 18 moderate sodium level	The risk of soil alkalinization is significant in fine-textured soils with high cation exchange capacity, especially under low leaching conditions. This water can be used on coarse-textured soils or organic soils with good permeability.
C3	18 < SAR ≤ 26 High sodium level	Water that may cause harmful alkalinity in most soils, except in those with low clay content. Its use requires special management measures ensuring good drainage and high leaching. The addition of organic matter or chemical amendments is often necessary.
C4	SAR > 26 very high sodium level	Water generally unsuitable for irrigation due to the high risk of alkalinization. Such water may be used for irrigation only if its salinity allows calcium addition or if the soil already contains sufficient calcium.

The temporal evolution of the Water Quality Index, characterized by a deterioration in 2022 followed by a marked improvement in 2024, reflects the dynamic balance between anthropogenic pressures and the natural attenuation capacity of the soil-aquifer system. Similar recovery patterns have been observed in other alluvial basins where pollutant inputs are moderated and biogeochemical attenuation processes remain effective (Table 7). This finding reinforces a central principle of sustainable groundwater management: preserving the natural filtering and buffering functions of soils and aquifers is as critical as controlling contaminant sources themselves.

Although the hydrochemical signature of the Boussellam aquifer is shaped by local geological, hydrological, and land-use conditions, the governing processes identified (climate-driven variability, cumulative anthropogenic loading, geochemically induced infrastructure constraints, and the interplay between pollution and natural attenuation) are broadly applicable to alluvial aquifers in semi-arid regions worldwide. As such, the present study contributes transferable insights for the long-term management and protection of groundwater resources under increasing climatic and anthropogenic stress.

CONCLUSIONS

The hydrochemical assessment of groundwater from the Oued Boussellam alluvial aquifer provides valuable insights into the processes governing water quality and its suitability for human and agricultural uses. The results confirm that the groundwater exhibits a predominantly alkaline character with moderate to high mineralization, controlled by natural geochemical interactions such as carbonate and sulfate dissolution and cation exchange. Despite minor spatial and temporal variations, the overall chemical composition has remained relatively stable over the study period (2020–2024), suggesting balanced recharge and limited external contamination.

The Water Quality Index classification indicates that most samples range from good to poor quality, confirming general suitability for irrigation and, in some cases, for domestic use following basic treatment. However, localized increases in nitrate and chloride concentrations point to anthropogenic influences, primarily agricultural activities and wastewater infiltration. The irrigation assessment highlights a persistent salinity hazard (S1C3 class), which could impair soil structure and crop yields if not properly managed. Implementing appropriate mitigation measures, such as improved drainage, regular soil leaching, and organic amendments, is therefore essential.

The groundwater of the BUR remains a vital resource for the region's socio-economic development. Yet, its long-term sustainability depends on integrated management strategies that combine regular hydrochemical monitoring, controlled fertilizer use, and protection of recharge zones. Continued surveillance of both natural and human-induced changes is crucial to ensure the preservation of groundwater quality and the resilience of this important aquifer system.

Authors' contribution

ZB. contributed to the conception of the study, data acquisition, and interpretation of the results. AM. participated in the data processing, statistical analysis, and drafting of the manuscript. RH. supervised the research work, contributed to the geological interpretation, and critically revised the manuscript for intellectual content. All authors have read and approved the final version of the manuscript.

Acknowledgments

This study was carried out under the supervision of IAWRSMB-Tunisia and the Laboratory of Applied Research in Engineering Geology, Geotechnics, Water Sciences, and Environment at Farhat Abbas University, Setif, Algeria. We also wish to express our deep gratitude to the editor and reviewers for their insightful comments and suggestions, which have greatly enhanced the quality of this manuscript.

Funding

This research did not receive any external funding.

Data Availability Statement

No new data were generated for this study.

Conflicts of Interest

The authors declare no conflicts of interest.

REFERENCES

Aher, D.N., Kele, V.D., Malwade, K.D., Shelke, M.D., 2016. Lake Water Quality Indexing to Identify Suitable Sites for Household Utility: A Case Study Jambhulwadi Lake; Pune (MS). International Journal of Engineering Research and Applications, 6, 16–21.

Benmarce, K., Hadji, R., Hamed, Y., Zahri, F., Zighmi, K., Hamad, A., Gentilucci, M., Ncibi, K., Besser, H., 2023. Hydrogeological and water quality analysis of thermal springs in the Guelma region of North-Eastern Algeria: A study using hydrochemical, statistical, and isotopic approaches. Journal of African Earth Sciences 205, Article 105011.

Benmarce, K., Zighmi, K., Hadji, R., Hamed, Y., Gentilucci, M., Barbieri, M., Pambianchi, G., 2024. Integration of GIS and Water-Quality Index for Preliminary Assessment of Groundwater Suitability for Human Consumption and Irrigation in Semi-Arid Region. Hydrology 11, 71. https://doi.org/10.3390/ hydrology11050071.

Bensoltane, M.A., Zeghadnia, L., Hadji, R., 2021. Physicochemical Characterization of Drinking Water Quality of the Communal Water Distribution Network in Souk Ahras City/Algeria. Civil Engineering Research Journal, 12(02), Article 555834.

Brahmi, S., Baali, F., Hadji, R., Brahmi, S., Hamad, A., Rahal, O., … Hamed, Y., 2021. Assessment of groundwater and soil pollution by leachate using electrical resistivity and induced polarization imaging survey, case of Tebessa municipal landfill, NE Algeria. Arabian Journal of Geosciences 14 (4), 1–13.

Brown, R.M., McClelland, N.I., Deininger, R.A., Tozer, R.G., 1970. A water quality index-do we dare. Water & Sewage Works 117(10), 339–343.

Charrouf, N., Zighmi, K., Amel, M., Benmarce, K., Hadji, R., Hamed, Y., Gentilucci, M., Farid, Z., 2025. Assessing climate change impacts on vegetation and water dynamics in semi-arid watersheds using remote sensing techniques. Studia Quaternaria 42, 61–73.

Chaturvedi, M.K., Bassin, J.K., 2010. Assessing the water quality index of water treatment plant and bore wells, in Delhi, India. Environmental monitoring and assessment 163(1), 449–453.

Chougar, R., Baalı, F., Hadji, R., Ghrieb, L., Hamad, A., Hamed, Y., 2024. Assessing groundwater quality in semiarid conditions: a geographic information systems-integrated approach using water quality index. Bulletin of the Mineral Research and Exploration 174, 129–143.

Durand, J.H., 1982. Irrigable Soils (340 p). PUF-Paris.

Giridharan, L., Venugopal, T., Jayaprakash, M., 2010. Identification and evaluation of hydrogeochemical processes on river Cooum, South India. Environmental monitoring and assessment 162(1), 277–289.

Hamed Y., Gentilucci M., Jallouli H., Ncibi K., Hadji R., Jraba A., Mlayeh A., Elimame Elaloui E., 2025b. Radiological environmental monitoring of groundwater around phosphate deposits in North Africa-Southern Tunisia: Geochemical, Environmental and

Health Factors. Acque Sotterranee – Italian Journal of Groundwater 14(1), 27–45. https://doi.org/10.7343/as-2025-809

Hamed, Y., Hadji, R., Ahmadi, R., Ayadi, Y., Shuhab, K., Pulido-Bosch, A., 2024a. Hydrogeological investigation of karst aquifers using an integrated geomorphological, geochemical, GIS, and remote sensing techniques (Southern Mediterranean Basin-Tunisia). Environment, development and sustainability 26(3), 6943–6975.

Hamed, Y., Jallouli, H., Khelifi, F., Garbaya, H., Hadji, R., Elaloui, E., 2025a. Radioactivity of the unconventional uranium resources from phosphate rock in Tunisia-remediation strategies. Euro-Mediterranean Journal for Environmental Integration 10, 5045–5062.

Hamed, Y., Khelifi, F., Houda, B., Sâad, A. B., Ncibi, K., Hadji, R., melki, A., Hamad, A., 2023. Phosphate mining pollution in southern Tunisia: environmental, epidemiological, and socioeconomic investigation. Environment, Development and Sustainability 25(11), 13619–13636.

Hamed, Y., Gentilucci, M., Mokadem, N., Khalil, R., Ayadi, Y., Hadji, R., Elaloui, E., 2024b. Assessment and Mitigation of Groundwater Contamination from Phosphate Mining in Tunisia: Geochemical and Radiological Analysis. Hydrology 11, Article 84. https://doi.org/10.3390/ hydrology11060084

Horton, R.K., 1965. An Index Number System for Water Quality Rating. Journal of Water Pollution Control Federation 37, 300–306.

Kannel, P.R., Lee, S., Lee, Y.S., Kanel, S.R., Khan, S.P., 2007. Application of water quality indices and dissolved oxygen as indicators for river water classification and urban impact assessment. Environmental monitoring and assessment 132(1), 93–110.

Kazi, T.G., Arain, M.B., Jamali, M.K., Jalbani, N., Afridi, H.I., Sarfraz, R.A., Baig, J.A., Shah, A.Q., 2009. Assessment of water quality of polluted lake using multivariate statistical techniques: A case study. Ecotoxicology and environmental safety 72(2), 301–309.

Möller, T., Kotta, J., Martin, G., 2009. Effect of observation method on the perception of community structure and water quality in a brackish water ecosystem. Marine Ecology 30, 105–112.

Ncibi, K., Hadji, R., Hamdi, M., Mokadem, N., Abbes, M., Khelifi, F., Zighmi, K., Hamed, Y., 2020. Application of the analytic hierarchy process to weight the criteria used to determine the Water Quality Index of groundwater in the northeastern basin of the Sidi Bouzid region, Central Tunisia. Euro-Mediterranean Journal for Environmental Integration 5, Article 19.

Nekkoub, A., Baali, F., Hadji, R., Hamed, Y., 2020. The EPIK multi-attribute method for intrinsic vulnerability assessment of karstic aquifer under semi-arid climatic conditions, case of Cheria Plateau, NE Algeria. Arabian Journal of Geosciences 13, 1–15.

Ouyang, Y., 2005. Evaluation of river water quality monitoring stations by principal component analysis. Water research 39(12), 2621–2635.

Savornin, J., 1920. Etude géologique de la région du Hodna et du plateau sétifien. Ancienne maison bastide-Jourdan, Jules carbonel, imprimeiur-libraire de l'Université.

Schäffer, R., Dietz, A., 2023. Standardized Schoeller diagrams – A Matlab plotting tool. Grundwasser 28(4), 345–355.

Subramani, T., Rajmohan, N., Elango, L., 2010. Groundwater geochemistry and identification of hydrogeochemical processes in a hard rock region, Southern India. Environmental monitoring and assessment 162(1), 123–137.

Vila, J.M., 1980. La chaîne alpine de l'Algérie orientale et des confins algéro-tunisiens. These de Doctorat-es-sciences, Universite Pierre et Marie Curie.